Electronic Research Archive

https://www.aimspress.com/journal/era

ERA, 32(11): 6258–6275.
DOI: 10.3934/era.2024291
Received: 10 September 2024
Revised: 12 November 2024
Accepted: 13 November 2024
Published: 19 November 2024

Research article

Observer-based event triggering security load frequency control for power systems involving air conditioning loads

Xiaoming Wang[1], Yunlong Bai[2], Zhiyong Li[2], Wenguang Zhao[1] and Shixing Ding[3,*]

[1] Electric Power Research Institute, State Grid Anhui Electric Power Co., Ltd., Hefei, China
[2] State Grid Anhui Electric Power Co., Ltd., Hefei, China
[3] School of Electrical Engineering, Southeast University, Nanjing 210096, China

* **Correspondence:** Email: dingshixingseu@163.com.

Abstract: This paper presents a power system frequency control strategy that integrates an observer-based event-triggered mechanism (ETM) to defend against denial-of-service (DoS) attacks and accommodates the integration of renewable energy sources. The proposed strategy incorporates demand response by enabling air conditioning loads (ACs) to participate in frequency regulation, thereby enhancing system flexibility and stability. To address the challenges posed by limited network bandwidth and potential message blocking, the ETM minimizes communication while defending against DoS attacks. The stability of the closed-loop system is guaranteed by deriving an H_∞ stability criterion using the Lyapunov–Krasovskii function method, with controller parameters determined through linear matrix inequalities (LMIs). A two-area power system simulation is conducted to validate the feasibility and effectiveness of the proposed approach, demonstrating its ability to maintain stable frequency control under cyber-attack scenarios and varying renewable energy contributions.

Keywords: load frequency control; air conditioning loads; DoS attack; observer; event-triggering mechanism; H_∞ optimization

1. Introduction

Load frequency control (LFC) is significant for the safe and stable work of the power grids [1–3]. With the continuous breakthrough of new energy technology, new energy power generation methods are gradually combined with traditional power generation methods and the penetration rate of modern smart grids continues to increase. Wind power and photovoltaic power are the most widely used forms of new energy generation. However, wind energy and photovoltaic energy are characterized by dispersion, randomness, fluctuation and intermittency [4], which can affect the power grid, especially the frequency.

Usually, when the frequency of the power system fluctuates, the aggregator load changes its working state according to the scheduling instruction to prevent frequency fluctuation [5, 6]. Most dynamic demand control models have been with thermostatically controlled devices, with air conditioning loads (ACs) accounting for a huge percentage of them [7, 8]. However, most literature focused on how ACs can be controlled based on optimized thought, such as the method based on the load frequency modulation model [9]. Only a few studies have applied ACs to resolve external perturbations [10, 11].

With the progress of ultra-high voltage technology and the increasing proportion of new energy in power generation [12–14], the communication data between power grid systems has become more complex, which also increases the communication pressure between power grids. In recent years, there has been a growing interest in event-triggered mechanisms (ETM) due to their potential in reducing communication and computation resources while maintaining stability and performance in complex systems [15–19]. ETM is designed to trigger actions and update processes in a system only when certain predefined conditions, or events, are met rather than at fixed time intervals. This smart adaptive strategy is particularly beneficial for systems in which resources are constrained or in dynamic environments where unnecessary updates could be costly. Kazemy et al. [15] have addressed synchronization of master-slave neural networks under deception attacks using event-triggered output feedback control to enhance stability and resilience.

While considering the limited network resources, we should also consider the security problems faced by networked systems [20]. Especially in recent years, industrial open networks have been attacked frequently. At present, network attacks are mainly divided into denial-of-service (DoS) attacks and spoofing attacks. DoS attacks can cause the loss of transmitted data [21], while spoofing attacks are launched by attackers that attempt to disrupt the availability of data [22]. Foroush and Martinez [23] showed that the general security problem of networked is DoS attack, which attempts to transmit a large amount of invalid data and intentionally interfere with network communication resources. Persis and Tesi [24] proved that on the premise of ensuring the asymptotic stability of the system, and the average active time of DoS attacks cannot exceed a certain percentage. In recent years, the research on the security of event-triggered networked systems has made some progress [15].

Inspired by the analysis presented above, this paper explores the application of an observer-based ETM for secure LFC in power systems, with the aim of ensuring the safety and stability of the power system. Considering the inherent instability caused by the increasing penetration of renewable energy in the grid, we treat it as a perturbation. In addition, this study proposes the integration of AC demand response as a control strategy to effectively regulate system frequency fluctuations. Additionally, this paper addresses key challenges related to network bandwidth limitations and potential DoS attacks by incorporating the ETM. A novel aspect of this work is the application of ETM to the observer rather than directly to the system state to mitigate the complexity and impracticalities associated with direct state measurement in real-world applications. The contribution of this paper is as follows:

i) The volatility associated with renewable energy generation is modeled as a perturbation, accounting for its unpredictable nature in the power system. To enhance the LFC, ACs demand response is incorporated as an effective tool to dynamically adjust the system's frequency in response to fluctuating generation conditions, thereby improving overall system resilience.

ii) In contrast to conventional ETM that rely on direct measurement of system states, this paper introduces an observer-based ETM. By using an observer to estimate system states, this approach

avoids the challenges and limitations of directly measuring these values, offering a practical solution for real-time control in large-scale, decentralized power networks.

Notations. $U > 0$ means the matrix U is positive definite. $*$ stands for the corresponding symmetric term in the matrix. $diag\{\cdots\}$ stands for diagonal matrix.

2. Problem formulation

2.1. Model description

First, considering the random disturbance of wind power and photovoltaic power generation, a multi-area smart grid control model is established with ACs participating in grid frequency regulation, as shown in Figure 1 [25]. System parameters and meanings are shown in Table 1, where $k_{aci} = \frac{m_i c_{pi} k}{\text{EER}}$.

According to Figure 1, we can obtain

$$\begin{cases} \Delta\dot{f}_i = \dfrac{1}{M_i}(\Delta P_{mi} + \Delta P_{vi} - \Delta P_{tie-i} - \Delta P_{aci} - \Delta P_{Li} - D_i\Delta f_i) \\ \Delta\dot{P}_{tie-i}(t) = 2\pi\left(T_{ii}\Delta f_i - \sum_{j=1,j\neq i}^{n} T_{ij}\Delta f_j\right) \\ \Delta\dot{P}_{mi} = \dfrac{1}{T_{ti}}(\Delta P_{vi} - \Delta P_{mi}) \\ \Delta\dot{P}_{vi} = \dfrac{1}{T_{gi}}(u - \Delta P_{vi} - \dfrac{\Delta f_i}{R_i}) \\ \Delta\dot{P}_{Wi} = \dfrac{1}{T_{Wi}}(\Delta P_{wind,i} - \Delta P_{Wi}) \\ \Delta\dot{P}_{Si} = \dfrac{1}{T_{PCi}}(\Delta P_{solar,i} - \Delta P_{Si}) \\ \Delta\dot{P}_{aci} = (0.5k_{aci} - D_{aci}D_i)\Delta f_i + D_{aci}(\Delta P_{mi} + \Delta P_{Wi} - \Delta P_{tie-i} - \Delta P_{aci} - \Delta P_{Li}) \\ ACE_i = \beta_i\Delta f_i + \Delta P_{tie-i} \end{cases}, \tag{2.1}$$

where $D_{aci} = \frac{2\pi d_{aci}}{M_i}$, $T_{ii} = \sum_{j=1,j\neq i}^{n} T_{ij}$, $i, j = 1, 2, \ldots, n$. Define

$$\mathrm{x}_i(\mathrm{t}) = \begin{bmatrix} \Delta f_i & \Delta P_{tie-i} & \Delta P_{mi} & \Delta P_{vi} & \Delta P_{Wi} & \Delta P_{Si} & \Delta P_{aci} \end{bmatrix}^T,$$

$$\omega_i(\mathrm{t}) = \begin{bmatrix} \Delta P_{Li} & \Delta P_{wind,i} & \Delta P_{solar,i} \end{bmatrix}^T, \mathrm{y}(\mathrm{t}) = ACE_i.$$

Then, we can obtain that

$$\begin{cases} \dot{\mathrm{x}}_i(\mathrm{t}) = \mathbb{A}_{ii}\mathrm{x}_i(\mathrm{t}) + \mathbb{B}_i\mathrm{u}(\mathrm{t}) + \mathbb{F}_i\omega_i(\mathrm{t}) - \sum_{j=1,j\neq i}^{n} \mathbb{A}_{ij}\mathrm{x}_j(\mathrm{t}) \\ \mathrm{y}_i(\mathrm{t}) = \mathbb{C}_i\mathrm{x}_i(\mathrm{t}) \end{cases}, \tag{2.2}$$

where

$$\mathbb{A}_{ii} = \begin{bmatrix} -\frac{D_i}{M_i} & -\frac{1}{M_i} & \frac{1}{M_i} & 0 & \frac{1}{M_i} & \frac{1}{M_i} & -\frac{1}{M_i} \\ 2\pi \sum_{j=1, j\neq i}^{N} T_{ij} & 0 & 0 & 0 & 0 & 0 & 0 \\ 0 & 0 & -\frac{1}{T_{ii}} & \frac{1}{T_{ii}} & 0 & 0 & 0 \\ -\frac{1}{R_i T_{gi}} & 0 & 0 & -\frac{1}{T_{gi}} & 0 & 0 & 0 \\ 0 & 0 & 0 & 0 & -\frac{1}{T_{Wi}} & 0 & 0 \\ 0 & 0 & 0 & 0 & 0 & -\frac{1}{T_{PCi}} & 0 \\ 0.5k_{aci} - D_{aci}D_i & -D_{aci} & D_{aci} & 0 & D_{aci} & D_{aci} & -D_{aci} \end{bmatrix}, \mathbb{B}_i = \begin{bmatrix} 0 \\ 0 \\ 0 \\ \frac{1}{T_{gi}} \\ 0 \\ 0 \\ 0 \end{bmatrix},$$

$$\mathbb{F}_i = \begin{bmatrix} -\frac{1}{M_i} & 0 & 0 \\ 0 & 0 & 0 \\ 0 & 0 & 0 \\ 0 & 0 & 0 \\ 0 & \frac{1}{T_{Wi}} & 0 \\ 0 & 0 & \frac{1}{T_{PCi}} \\ -D_{aci} & 0 & 0 \end{bmatrix}, \mathbb{C}_i = \begin{bmatrix} \beta_i \\ 1 \\ 0 \\ 0 \\ 0 \\ 0 \\ 0 \end{bmatrix}^T, \mathbb{A}_{ij} = [(2,1) = -2\pi T_{ij}].$$

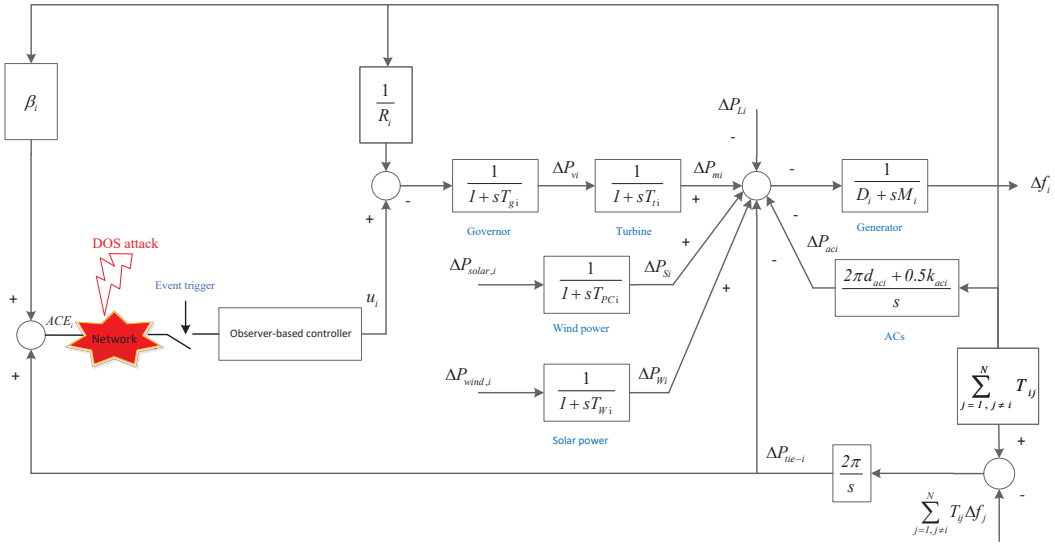

Figure 1. LFC diagram of the i area.

From (2.2), the state-space form of multi-area ACs LFC model can be described as

$$\begin{cases} \dot{x}(t) = & \mathcal{A}x(t) + \mathcal{B}u(t) + \mathcal{F}\omega(t) \\ y(t) = & Cx(t) \end{cases}, \tag{2.3}$$

with

$$\mathcal{A} = \begin{bmatrix} \mathbb{A}_{11} & \mathbb{A}_{12} & \dots & \mathbb{A}_{1n} \\ \mathbb{A}_{21} & \mathbb{A}_{22} & \dots & \mathbb{A}_{2n} \\ \vdots & \vdots & \ddots & \vdots \\ \mathbb{A}_{n1} & \mathbb{A}_{n2} & \dots & \mathbb{A}_{nn} \end{bmatrix},$$

$$C = diag\{\mathbb{C}_1, \mathbb{C}_2, \dots, \mathbb{C}_n\}, \mathcal{B} = diag\{\mathbb{B}_1, \mathbb{B}_2, \dots, \mathbb{B}_n\}, \mathcal{F} = diag\{\mathbb{F}_1, \mathbb{F}_2, \dots, \mathbb{F}_n\},$$

$$\mathrm{x(t)} = \begin{bmatrix} \mathrm{x}_1(\mathrm{t}) & \mathrm{x}_2(\mathrm{t}) & \dots & \mathrm{x}_n(\mathrm{t}) \end{bmatrix}^T, \mathrm{y(t)} = \begin{bmatrix} \mathrm{y}_1(\mathrm{t}) & \mathrm{y}_2(\mathrm{t}) & \dots & \mathrm{y}_n(\mathrm{t}) \end{bmatrix}^T,$$

$$\omega(\mathrm{t}) = \begin{bmatrix} \omega_1^T(\mathrm{t}) & \omega_2^T(\mathrm{t}) & \dots & \omega_n^T(\mathrm{t}) \end{bmatrix}^T, \mathrm{u(t)} = \begin{bmatrix} \mathrm{u}_1(\mathrm{t}) & \mathrm{u}_2(\mathrm{t}) & \dots & \mathrm{u}_n(\mathrm{t}) \end{bmatrix}^T.$$

Table 1. System parameters and meanings in Figure 1.

Symbol	Name
Δf_i	frequency deviation
ΔP_{mi}	generation mechanical output deviation
ΔP_{tie-i}	tie-line active power deviation
$\Delta P_{wind,i}$	wind power deviation
ΔP_{Wi}	output of wind turbine generator deviation
$\Delta P_{solar,i}$	solar power deviation
ΔP_{Si}	the deviations of output of photovoltaic
ΔP_{aci}	the deviations of output of ACs
ΔP_{vi}	valve position deviation
ACE_i	area control error
T_{gi}	governor time constant
T_{ti}	turbine time constant
D_i	the generator unit damping coefficient
T_{Wi}	the wind turbine generator time constant
T_{PVi}	the photovoltaic time constant
T_{ij}	lie-line synchronizing coefficient between the ith and jth control area
d_{aci}	the damping coefficient
k_{aci}	the combined integral gain
β_i	frequency bias factor
EER	energy efficiency ratio
c_{pi}	specific heat capacity of the air
R_i	the speed drop
k	gain factor in the smart thermostat
M_i	the moment of inertia of the generator unit
m_i	the mass of air flow

2.2. Full-order state observer

The full-order state observer is constructed as

$$\begin{cases} \dot{\hat{\mathrm{x}}}(\mathrm{t}) = \mathcal{A}\hat{\mathrm{x}}(\mathrm{t}) + \mathcal{B}\mathrm{u}(\mathrm{t}) + \mathcal{L}(\mathrm{y}(\mathrm{t}) - \hat{\mathrm{y}}(\mathrm{t})) \\ \hat{\mathrm{y}}(\mathrm{t}) = C\hat{\mathrm{x}}(\mathrm{t}) \end{cases}, \tag{2.4}$$

where $\hat{\mathrm{y}}(\mathrm{t})$ is the observer output; $\hat{\mathrm{x}}(\mathrm{t})$ is the observer state and $\mathcal{L}$ is the observer gain to be solved.

2.3. Observer-based ETM under DoS attacks

In this paper, inspired by [26, 27], and periodic event-triggered control schemes [28], we select the ETM activations:

$$\begin{aligned} \mathrm{t}_{k+1} &= \mathrm{t}_k + min\{lh | f[\hat{\mathrm{x}}(\mathrm{t}_k), \zeta(\mathrm{t})] \leq 0\}, \\ f[\hat{\mathrm{x}}(\mathrm{t}_k), \zeta(t)] &= \zeta^T(\mathrm{t})\mathrm{V}\zeta(\mathrm{t}) - \sigma\hat{\mathrm{x}}^T(\mathrm{t}_k)\mathrm{V}\hat{\mathrm{x}}(\mathrm{t}_k), \\ i_k h &= \mathrm{t}_k + lh, \end{aligned} \tag{2.5}$$

where the difference between the most recent data sample and the current one is referred to as $\zeta(\mathrm{t})$, i.e., $\zeta(\mathrm{t}) = \hat{\mathrm{x}}(\mathrm{t}_k + lh) - \hat{\mathrm{x}}(\mathrm{t}_k)$, lh is the intervals between t_k and t_{k+1}, $l \in N, i_k h \in (\mathrm{t}_k, \mathrm{t}_{k+1}]$, and σ is a threshold parameter.

Remark 1. *Unlike traditional ETM that rely on state controllers, this paper introduces a novel approach using observer packets for triggering. This approach leverages the observer pattern, which offers significant advantages in terms of modularity and flexibility. Specifically, the observer pattern enables the seamless addition of new observers to the system without disrupting or modifying other components, ensuring a high degree of decoupling. Similarly, the observed object itself is free to evolve or modify its internal implementation without causing any adverse effects on the observers.*

In addition, consider the time-varying delay d_k caused by the network between the observer and the event generator [29]. Define $d(\mathrm{t})$ as follows:

$$d(\mathrm{t}) = \begin{cases} \mathrm{t} - \mathrm{t}_k, & \mathrm{t} \in I_1 \\ \mathrm{t} - \mathrm{t}_k - lh, & \mathrm{t} \in I_2^l, l = 1, 2, \ldots, m-1 \\ \mathrm{t} - \mathrm{t}_k - mh, & \mathrm{t} \in I_3 \end{cases}, d_m \leq d(\mathrm{t}) \leq d_M, \tag{2.6}$$

where $I_1 = [\mathrm{t}_k + d_k, \mathrm{t}_k + d_k + h)$, $I_2^l = [\mathrm{t}_k + d_k + lh, \mathrm{t}_k + d_k + lh + h)$, $I_2 = \cup_{l=1}^{l=m-1} I_2^l$, $I_3 = [\mathrm{t}_k + d_k + mh, \mathrm{t}_{k+1} + d_{k+1})$, $[\mathrm{t}_k + d_k, \mathrm{t}_{k+1} + d_{k+1}) = I_1 \cup I_2 \cup I_3$. Moreover, $\hat{\mathrm{x}}(\mathrm{t}_k)$ and $\hat{\mathrm{x}}(\mathrm{t}_k + \iota h)$ with $\iota = 1, 2, \ldots, m$ satisfy (2.5); d_m (d_M) denotes the lower (upper) bound on the time delay.

Remark 2. *In a multi-area power system, data transmission is routine, but network delays are inevitable. These delays can arise from factors like communication latency or network congestion, and if ignored, they may compromise the accuracy of the measured data. In this study, we define the delay as d_k and focus on the case where d_k is shorter than the sampling interval. This ensures that the integrity of the data sequence is preserved, with each measurement arriving and being processed within its designated sampling period.*

For $t \in [\mathrm{t}_k + d_k, \mathrm{t}_{k+1} + d_{k+1})$, we can define

$$\zeta(\mathrm{t}) = \begin{cases} 0, & t \in I_1 \\ \hat{\mathrm{x}}(\mathrm{t}_k + lh) - \hat{\mathrm{x}}(\mathrm{t}_k), & \mathrm{t} \in I_2^l \\ \hat{\mathrm{x}}(\mathrm{t}_k + mh) - \hat{\mathrm{x}}(\mathrm{t}_k), & t \in I_3 \end{cases}. \tag{2.7}$$

In what follows, inspired by [30], the observer-based ETM u(t) can be written as

$$\mathrm{u}(\mathrm{t}) = \mathcal{K}\hat{\mathrm{x}}(\mathrm{t}_k),$$

where $\mathcal{K}$ is the control gain matrix.

Based on (2.6) and (2.7), the observer-based ETM u(t) can be rewritten as

$$\mathrm{u}(\mathrm{t}) = \mathcal{K}\hat{\mathrm{x}}(\mathrm{t}_k) = \mathcal{K}(\hat{\mathrm{x}}(\mathrm{t} - d(\mathrm{t})) - \zeta(\mathrm{t})). \tag{2.8}$$

For a DOS attack in a network, define $\tau(i_k h)$ as the attack state, $\tau(i_k h) = 1$ as the attack occurred, and $\tau(i_k h) = 0$ as the attack did not occur. In a typical power system, most DoS attacks fail to achieve their purpose, and only a fraction of these attacks cause notable disruptions. We divide DoS attacks into the following four types:

$$\begin{cases} \begin{cases} \tau(i_k h) = 0, & \mathrm{t} \in (\mathrm{t}_k, \mathrm{t}_{k+1}) \quad : \quad no \quad DOS \quad attack \\ \tau(i_k h) = 0, & t \in (\mathrm{t}_{k+1}, \mathrm{t}_{k+1}^{DOS}) \quad : \quad no \quad DOS \quad attack \end{cases} \\ \begin{cases} \tau(i_k h) = 1, & \mathrm{t} \in (\mathrm{t}_k, \mathrm{t}_{k+1}) \quad : \quad ineffective \quad Dos \quad attack \\ \tau(i_k h) = 1, & t \in (\mathrm{t}_{k+1}, \mathrm{t}_{k+1}^{DOS}) \quad : \quad effective \quad DoS \quad attacks \end{cases} \end{cases}. \tag{2.9}$$

In addition, the energy of general DoS attacks is limited. Facing such attacks, we introduce elastic variable $\zeta_{DoS}(\mathrm{t})$ on the event triggering mechanism to represent the packet loss and delay caused by DoS attacks on the system [31]. We can obtain

$$\mathrm{t}_{k+1}^{DoS} = \mathrm{t}_k + min\{lh | f[\hat{\mathrm{x}}(\mathrm{t}_k), \zeta(\mathrm{t})] - \tau(i_k h)\zeta_{DoS}^T(\mathrm{t}) \mathrm{V} \zeta_{DoS}(\mathrm{t}) \geq 0\}, \tag{2.10}$$

$$\mathrm{t}_{k+1}^{DoS} - \mathrm{t}_{k+1} = \Delta_{\mathrm{t}_{k+1}}^{DoS} \leq \Delta_{DoS}, \tag{2.11}$$

where Δ_{DoS} denotes the longest duration of a DoS attack and t_{k+1}^{DoS} refers to an upcoming sampling moment affected by DoS.

2.4. Modeling augmented systems

Substituting (2.8) into sysetm (2.3) yields

$$\begin{cases} \dot{\mathrm{x}}(\mathrm{t}) & = \mathcal{A}\mathrm{x}(\mathrm{t}) + \mathcal{B}\mathcal{K}\hat{\mathrm{x}}(\mathrm{t} - d(\mathrm{t})) - \mathcal{B}\mathcal{K}\zeta(\mathrm{t}) + \mathcal{F}\omega(\mathrm{t}) \\ \mathrm{y}(\mathrm{t}) & = \mathcal{C}\mathrm{x}(\mathrm{t}) \end{cases}. \tag{2.12}$$

Substituting (2.8) into system (2.4) yields

$$\dot{\hat{\mathrm{x}}}(\mathrm{t}) = \mathcal{A}\hat{\mathrm{x}}(\mathrm{t}) + \mathcal{B}\mathcal{K}\hat{\mathrm{x}}(\mathrm{t} - d(\mathrm{t})) - \mathcal{B}\mathcal{K}\zeta(t) + \mathcal{L}\mathcal{C}(\mathrm{x}(\mathrm{t}) - \hat{\mathrm{x}}(\mathrm{t})). \tag{2.13}$$

Define the state error as $\delta(t) = x(t) - \hat{x}(t)$, then

$$\dot{\delta}(t) = (\mathcal{A} - \mathcal{L}C)\delta(t) + \mathcal{F}\omega(t). \tag{2.14}$$

Define the augmented state as $\tilde{x}^T(t) = \begin{bmatrix} x^T(t) & \delta^T(t) \end{bmatrix}$, the augmented system is

$$\begin{cases} \dot{\tilde{x}}(t) = \mathcal{A}_1\tilde{x}(t) + \mathcal{A}_2\tilde{x}(t - d(t)) + \mathcal{B}_1\zeta(t) + \mathcal{B}_2\omega(t) \\ y(t) = C\mathcal{E}\tilde{x}(t) \end{cases}, \tag{2.15}$$

where

$$\mathcal{A}_1 = \begin{bmatrix} \mathcal{A} & \mathbf{0} \\ \mathbf{0} & \mathcal{A} - \mathcal{L}C \end{bmatrix}, \mathcal{A}_2 = \begin{bmatrix} \mathbf{0} & \mathcal{B}\mathcal{K} \\ \mathbf{0} & \mathbf{0} \end{bmatrix}, \mathcal{B}_1 = \begin{bmatrix} -\mathcal{B}\mathcal{K} \\ \mathbf{0} \end{bmatrix}, \mathcal{B}_2 = \begin{bmatrix} \mathcal{F} \\ \mathcal{F} \end{bmatrix}, \mathcal{E} = \begin{bmatrix} I \\ \mathbf{0} \end{bmatrix}^T.$$

Definition 1. *[32, 33] For an arbitrary initial condition, given $\gamma > 0$, the augmented system (2.15) is thought to be stable with H_∞ performance if the following two conditions are met:*
1) for $\omega(t) = 0$, the system is asymptotically stable;
2) for $\omega(t) \in \ell_2[0, \infty)$, the following condition is satisfied:

$$\| y(t) \|_2 \leq \gamma \| \omega(t) \|_2 .$$

Lemma 1. *[34] For a given time delays constant d_m and d_M satisfying $d(t) \in [d_m, d_M]$, for $d_M > d_m > 0$, there exist matrices R_2 and H when*

$$\begin{bmatrix} \mathsf{R}_2 & \mathsf{H} \\ * & \mathsf{R}_2 \end{bmatrix} > 0$$

for which the following inequality holds:

$$\begin{aligned} &-(d_M - d_m)\int_{t-d_M}^{t-d_m} \dot{\tilde{x}}^T(s)\mathsf{R}_2\dot{\tilde{x}}(s)ds \\ &\leq \begin{bmatrix} \tilde{x}^T(t - d_m) \\ \tilde{x}^T(t - d(t)) \\ \tilde{x}^T(t - d_M) \end{bmatrix}^T \begin{bmatrix} -\mathsf{R}_2 & \mathsf{R}_2 - \mathsf{H} & \mathsf{H} \\ * & -2\mathsf{R}_2 + \mathsf{H} + \mathsf{H}^T & \mathsf{R}_2 - \mathsf{H} \\ * & * & -\mathsf{R}_2 \end{bmatrix} \begin{bmatrix} \tilde{x}(t - d_m) \\ \tilde{x}(t - d(t)) \\ \tilde{x}(t - d_M) \end{bmatrix}. \end{aligned}$$

3. Main results

Two theorems are given in this section. Theorem 1 illustrates the stability and H_∞ performance of the augmented system, and Theorem 2 gives the design of an observer-based controller.

Theorem 1. *For some given positive constants σ , d_m and d_M, the augmented system (2.15) is asymptotically stable with an H_∞ performance index γ , if there exist positive definite matrices P, Q_1, Q_2, R_1, R_2, H and V with appropriate dimensions such that*

$$\Omega = \begin{bmatrix} \Omega_{11} & \Omega_{12} \\ * & \Omega_{22} \end{bmatrix} < 0, \tag{3.1}$$

$$\begin{bmatrix} \mathsf{R}_2 & \mathsf{H} \\ * & \mathsf{R}_2 \end{bmatrix} > 0, \tag{3.2}$$

where

$$\Omega_{11} = \begin{bmatrix} \Pi_{11} & \mathsf{R}_1 & \mathsf{P}\mathcal{A}_2 & \mathbf{0} & \mathsf{P}\mathcal{B}_1 & \mathsf{P}\mathcal{B}_2 \\ * & \Pi_{22} & \mathsf{R}_2 - \mathsf{H} & \mathsf{H} & \mathbf{0} & \mathbf{0} \\ * & * & \Pi_{33} & \mathsf{R}_2 - \mathsf{H} & \mathbf{0} & \mathbf{0} \\ * & * & * & -\mathsf{Q}_2 - \mathsf{R}_2 & \mathbf{0} & \mathbf{0} \\ * & * & * & * & -\mathsf{V} & \mathbf{0} \\ * & * & * & * & * & -\gamma^2 I \end{bmatrix},$$

$$\Omega_{12} = \begin{bmatrix} d_m\mathcal{A}_1^T & (d_M - d_m)\mathcal{A}_1^T & (\mathcal{CE})^T & \mathbf{0} \\ \mathbf{0} & \mathbf{0} & \mathbf{0} & \mathbf{0} \\ d_m\mathcal{A}_2^T & (d_M - d_m)\mathcal{A}_2^T & \mathbf{0} & \sigma\Pi_4^T \\ \mathbf{0} & \mathbf{0} & \mathbf{0} & \mathbf{0} \\ d_m\mathcal{B}_1^T & (d_M - d_m)\mathcal{B}_1^T & \mathbf{0} & -\sigma I \\ d_m\mathcal{B}_2^T & (d_M - d_m)\mathcal{B}_2^T & \mathbf{0} & \mathbf{0} \end{bmatrix},$$

$$\Omega_{22} = diag\{-\mathsf{R}_1^{-1}, -\mathsf{R}_2^{-1}, -I, -\sigma\mathsf{V}^{-1}\},$$

$$\Pi_{11} = \mathcal{A}_1^T\mathsf{P} + \mathsf{P}\mathcal{A}_1^T + \mathsf{Q}_1 + \mathsf{Q}_2 - \mathsf{R}_1,$$

$$\Pi_{22} = -\mathsf{Q}_1 - \mathsf{R}_1 - \mathsf{R}_2,$$

$$\Pi_{33} = -2\mathsf{R}_2 + \mathsf{H} + \mathsf{H}^T,$$

$$\Pi_4 = \begin{bmatrix} I & -I \end{bmatrix}.$$

Proof. Select Lyapunov function as

$$\begin{aligned} \mathbb{V}(\mathrm{t}) =& \tilde{\mathrm{x}}^T(\mathrm{t})\mathsf{P}\tilde{\mathrm{x}}(\mathrm{t}) + \int_{\mathrm{t}-d_m}^{\mathrm{t}} \tilde{\mathrm{x}}^T(s)\mathsf{Q}_1\tilde{\mathrm{x}}(s)ds + \int_{\mathrm{t}-d_M}^{\mathrm{t}} \tilde{\mathrm{x}}^T(s)\mathsf{Q}_2\tilde{\mathrm{x}}(s)ds \\ &+ d_m \int_{\mathrm{t}-d_m}^{\mathrm{t}} \int_{s}^{\mathrm{t}} \dot{\tilde{\mathrm{x}}}^T(v)\mathsf{R}_1\dot{\tilde{\mathrm{x}}}(v)dvds \\ &+ (d_M - d_m) \int_{-d_M}^{-d_m} \int_{\mathrm{t}-d_M}^{\mathrm{t}-d_m} \dot{\tilde{\mathrm{x}}}^T(v)\mathsf{R}_2\dot{\tilde{\mathrm{x}}}(v)dvds. \end{aligned}$$

From the augmented system (2.15) , we have

$$\begin{aligned} \dot{\mathbb{V}}(\mathrm{t}) =& \dot{\tilde{\mathrm{x}}}^T(\mathrm{t})\mathsf{P}\tilde{\mathrm{x}}(\mathrm{t}) + \tilde{\mathrm{x}}^T(\mathrm{t})\mathsf{P}\dot{\tilde{\mathrm{x}}}(\mathrm{t}) + \tilde{\mathrm{x}}^T(\mathrm{t})\mathsf{Q}_1\tilde{\mathrm{x}}(\mathrm{t}) - \tilde{\mathrm{x}}^T(\mathrm{t}-d_m)\mathsf{Q}_1\tilde{\mathrm{x}}(\mathrm{t}-d_m) \\ &+ \tilde{\mathrm{x}}^T(\mathrm{t})\mathsf{Q}_2\tilde{\mathrm{x}}(\mathrm{t}) - \tilde{\mathrm{x}}^T(\mathrm{t}-d_M)\mathsf{Q}_2\tilde{\mathrm{x}}(\mathrm{t}-d_M) + \dot{\tilde{\mathrm{x}}}^T(\mathrm{t})[d_m^2\mathsf{R}_1 + (d_M - d_m)^2\mathsf{R}_2]\dot{\tilde{\mathrm{x}}}(\mathrm{t}) \\ &- d_m \int_{\mathrm{t}-d_m}^{\mathrm{t}} \dot{\tilde{\mathrm{x}}}^T(s)\mathsf{R}_1\dot{\tilde{\mathrm{x}}}(s)ds - (d_M - d_m) \int_{\mathrm{t}-d_M}^{\mathrm{t}-d_m} \dot{\tilde{\mathrm{x}}}^T(s)\mathsf{R}_2\dot{\tilde{\mathrm{x}}}(s)ds. \end{aligned} \tag{3.3}$$

Using Jessen inequality, Lemma 1 and the Schur complement theorem, at the same time to join the event trigger condition, it can be concluded that

$$\begin{aligned} \dot{\mathbb{V}}(\mathrm{t}) + \mathrm{y}^T(\mathrm{t})\mathrm{y}(\mathrm{t}) - \gamma^2\omega^T(\mathrm{t})\omega(\mathrm{t}) &\le \xi^T(\mathrm{t})\{\Omega_{11} + \Gamma_1^T[d_m^2\mathsf{R}_1 + (d_M - d_m)^2\mathsf{R}_2]\Gamma_1 \\ &\quad + \Gamma_2^T\Gamma_2 + \Gamma_3^T\Gamma_3\}\xi(\mathrm{t}) \\ &\le \xi^T(\mathrm{t})\Omega\xi(\mathrm{t}), \end{aligned} \tag{3.4}$$

where

$$\xi^T(\mathrm{t}) = [\tilde{\mathrm{x}}(\mathrm{t}), \tilde{\mathrm{x}}(\mathrm{t}-d_m), \tilde{\mathrm{x}}(\mathrm{t}-d(t)), \tilde{\mathrm{x}}(\mathrm{t}-d_M), \zeta(t), \omega(\mathrm{t})],$$

$$\Gamma_1 = [\mathcal{A}_1, \mathbf{0}, \mathcal{A}_2, \mathbf{0}, \mathcal{B}_1, \mathcal{B}_2],$$

$$\Gamma_2 = [\mathcal{CE}, \mathbf{0}, \mathbf{0}, \mathbf{0}, \mathbf{0}, \mathbf{0}],$$

$$\Gamma_3 = [\mathbf{0}, \mathbf{0}, \sigma\Pi_4, \mathbf{0}, -\sigma I, \mathbf{0}].$$

Further, we achieve

$$\mathrm{y}^T(\mathrm{t})\mathrm{y}(\mathrm{t}) - \gamma^2\omega^T(\mathrm{t})\omega(\mathrm{t}) \leq -\dot{\mathbb{V}}(\mathrm{t}). \tag{3.5}$$

According to (3.4) and (3.5), the presence of $\lambda > 0$ ensures that $\dot{\mathbb{V}}(\mathrm{t}) < 0$ is satisfied when $\omega(\mathrm{t}) = 0$, and we can achieve $lim_{t\to\infty}\mathbb{V}(\mathrm{t}) = 0$.

By Definition 1, the augmented system (2.15) is asymptotically stable.

When $\omega(\mathrm{t}) \neq 0$, both sides of (3.5) integrate from 0 to $+\infty$,

$$\int_0^{+\infty} (\mathrm{y}^T(\mathrm{t})\mathrm{y}(\mathrm{t}) - \gamma^2\omega^T(\mathrm{t})\omega(\mathrm{t}))d\mathrm{t} \leq \mathbb{V}(0) - \mathbb{V}(+\infty).$$

At zero original condition, we obtain

$$\| \mathrm{y}(\mathrm{t}) \|_2 \leq \gamma \| \omega(\mathrm{t}) \|_2 .$$

Since $\Omega < 0$, there exists a proper positive ε so that

$$\xi^T(\mathrm{t})\Omega\xi(\mathrm{t}) \leq -\varepsilon\mathbb{V}(\mathrm{t}),$$

$$\begin{aligned}\dot{\mathbb{V}}(\mathrm{t}) + \mathrm{y}^T(\mathrm{t})\mathrm{y}(\mathrm{t}) - \gamma^2\omega^T(\mathrm{t})\omega(\mathrm{t}) &\leq \xi^T(\mathrm{t})\Omega\xi(\mathrm{t}) \\ &\leq -\varepsilon\mathbb{V}(\mathrm{t}) + \tau(i_k h)\zeta_{DoS}^T(\mathrm{t})\mathsf{V}\zeta_{DoS}(\mathrm{t}).\end{aligned}$$

Multiply the upper expression by $e^{\varepsilon \mathrm{t}}$ and integrate the result. Subsequently,

$$\begin{aligned}\mathbb{V}(\mathrm{t}) &\leq e^{\varepsilon\mathrm{t}}\mathbb{V}(0) + (1 - e^{-\varepsilon\mathrm{t}})\frac{\tau(i_k h)\zeta_{DoS}^T(\mathrm{t})\mathsf{V}\zeta_{DoS}(\mathrm{t})}{\varepsilon} \\ &\leq \mathbb{V}(0) + \frac{\tau(i_k h)\zeta_{DoS}^T(\mathrm{t})\mathsf{V}\zeta_{DoS}(\mathrm{t})}{\varepsilon}.\end{aligned}$$

It is evident that

$$\tilde{\mathrm{x}}^T(\mathrm{t})\mathsf{P}\tilde{\mathrm{x}}(\mathrm{t}) \leq \mathbb{V}(0) + \frac{\tau(i_k h)\zeta_{DoS}^T(\mathrm{t})\mathsf{V}\zeta_{DoS}(\mathrm{t})}{\varepsilon},$$

$$\| \tilde{\mathrm{x}}(\mathrm{t}) \| \leq \sqrt{\frac{\mathbb{V}(0) + \frac{\tau(i_k h)\zeta_{DoS}^T(\mathrm{t})\mathsf{V}\zeta_{DoS}(\mathrm{t})}{\varepsilon}}{\lambda(\mathsf{P})}} = \Delta.$$

In the presence of an attack, the system's security performance bounds uniformly, with a degradation no greater than Δ. This finishes the proof.

Theorem 2. *For some given positive constants σ, d_m and d_M, the augmented system (2.15) is asymptotical stable with an H_∞ performance index γ , if there exist positive definite matrices X_i, Y, S, $\overline{\mathsf{Q}}_i$, $\overline{\mathsf{R}}_i$, $\overline{\mathsf{H}}$ and $\overline{\mathsf{V}}$ $(i = 1, 2)$ with appropriate dimensions such that*

$$\overline{\Omega} = \begin{bmatrix} \overline{\Omega}_{11} & \overline{\Omega}_{12} \\ * & \overline{\Omega}_{22} \end{bmatrix} < 0, \tag{3.6}$$

$$\begin{bmatrix} \overline{\mathsf{R}}_2 & \overline{\mathsf{H}} \\ * & \overline{\mathsf{R}}_2 \end{bmatrix} > 0, \tag{3.7}$$

where

$$\overline{\Omega}_{11} = \begin{bmatrix} \overline{\Pi}_{11} & \overline{\mathsf{R}}_1 & \Psi_1 & \mathbf{0} & \Psi_2 & \mathcal{B}_2 \\ * & \overline{\Pi}_{22} & \overline{\mathsf{R}}_2 - \overline{\mathsf{H}} & \overline{\mathsf{H}} & \mathbf{0} & \mathbf{0} \\ * & * & \overline{\Pi}_{33} & \overline{\mathsf{R}}_2 - \overline{\mathsf{H}} & \mathbf{0} & \mathbf{0} \\ * & * & * & -\overline{\mathsf{Q}}_2 - \overline{\mathsf{R}}_2 & \mathbf{0} & \mathbf{0} \\ * & * & * & * & -\overline{\mathsf{V}} & \mathbf{0} \\ * & * & * & * & * & -\gamma^2 I \end{bmatrix},$$

$$\overline{\Omega}_{12} = \begin{bmatrix} d_m\Psi_0^T & (d_M - d_m)\Psi_0^T & \Psi_3^T & \mathbf{0} \\ \mathbf{0} & \mathbf{0} & \mathbf{0} & \mathbf{0} \\ d_m\Psi_1^T & (d_M - d_m)\Psi_1^T & \mathbf{0} & \sigma\overline{\Pi}_4^T \\ \mathbf{0} & \mathbf{0} & \mathbf{0} & \mathbf{0} \\ d_m\Psi_2^T & (d_M - d_m)\Psi_2^T & \mathbf{0} & -\sigma\mathsf{X}_2 \\ d_m\mathcal{B}_2^T & (d_M - d_m)\mathcal{B}_2^T & \mathbf{0} & \mathbf{0} \end{bmatrix},$$

$$\overline{\Omega}_{22} = diag\{\overline{\mathsf{R}}_1 - 2\mathsf{X}, \overline{\mathsf{R}}_2 - 2\mathsf{X}, -I, \sigma(\overline{\mathsf{V}} - 2\mathsf{X}_2)\},$$

$$\Psi_0 = \begin{bmatrix} \mathcal{A}\mathsf{X}_1 & \mathbf{0} \\ \mathbf{0} & \mathcal{A}\mathsf{X}_2 - \mathsf{S}\mathcal{C} \end{bmatrix}, \Psi_1 = \begin{bmatrix} \mathbf{0} & \mathcal{B}\mathsf{Y} \\ \mathbf{0} & \mathbf{0} \end{bmatrix}, \Psi_2 = \begin{bmatrix} -\mathcal{B}\mathsf{Y} \\ \mathbf{0} \end{bmatrix}, \Psi_3 = \begin{bmatrix} \mathcal{C}\mathsf{X}_1 & \mathbf{0} \end{bmatrix},$$

$$\overline{\Pi}_{11} = \Psi_0 + \Psi_0^T + \overline{\mathsf{Q}}_1 + \overline{\mathsf{Q}}_2 - \overline{\mathsf{R}}_1, \overline{\Pi}_{22} = -\overline{\mathsf{Q}}_1 - \overline{\mathsf{R}}_1 - \overline{\mathsf{R}}_2,$$

$$\overline{\Pi}_{33} = -2\overline{\mathsf{R}}_2 + \overline{\mathsf{H}} + \overline{\mathsf{H}}^T, \overline{\Pi}_4 = \begin{bmatrix} \mathsf{X}_1 & -\mathsf{X}_2 \end{bmatrix},$$

$$\mathsf{X} = \begin{bmatrix} \mathsf{X}_1 & \mathbf{0} \\ * & \mathsf{X}_2 \end{bmatrix}.$$

The control coefficient matrix of the observer-based controller is shown by: $\mathcal{K} = \mathsf{Y}\mathsf{X}_2^{-1}$, $\mathcal{L} = \mathsf{S}\overline{\mathsf{X}}_2^{-1}$, with $\mathcal{C}\mathsf{X}_2 = \overline{\mathsf{X}}_2\mathcal{C}$.

Proof. Set $\mathsf{P} = \begin{bmatrix} \mathsf{P}_1 & \mathbf{0} \\ * & \mathsf{P}_2 \end{bmatrix}$ and define $\mathsf{X} = \mathsf{P}^{-1} = \begin{bmatrix} \mathsf{X}_1 & \mathbf{0} \\ * & \mathsf{X}_2 \end{bmatrix}$, $\overline{\mathsf{Q}}_i = \mathsf{X}^T\mathsf{Q}_i\mathsf{X}$, $\overline{\mathsf{R}}_i = \mathsf{X}^T\mathsf{R}_i\mathsf{X}$ $(i = 1, 2)$, $\overline{\mathsf{H}} = \mathsf{X}^T\mathsf{H}\mathsf{X}$, $\overline{\mathsf{V}} = \mathsf{X}_2{}^T\mathsf{V}\mathsf{X}_2$, $\mathsf{Y} = \mathcal{K}\mathsf{X}_2$, $\mathsf{S} = \mathcal{L}\overline{\mathsf{X}}_2$. For $\mathsf{X}_2 = \mathsf{W}\begin{bmatrix} \mathsf{X}_{21} & \mathbf{0} \\ * & \mathsf{X}_{22} \end{bmatrix}\mathsf{W}^T$, on the basis of [35], there exist $\overline{\mathsf{X}}_2 = \mathsf{M}\mathsf{N}\mathsf{X}_{22}\mathsf{N}^{-1}\mathsf{M}^T$ such that $\mathcal{C}\mathsf{X}_2 = \overline{\mathsf{X}}_2\mathcal{C}$.

Define $\Phi = diag\{\mathsf{X}, \mathsf{X}, \mathsf{X}, \mathsf{X}, \mathsf{X}_2, I, I, I, I, I\}$, then pre- and postmultiply Φ and its transpose on both sides of (3.1). It is easy to know that $-\mathsf{X}\overline{\mathsf{R}}_i^{-1}\mathsf{X} \le \overline{\mathsf{R}}_i - 2\mathsf{X}$, $(i = 1, 2)$, $-\mathsf{X}_2\overline{\mathsf{V}}^{-1}\mathsf{X}_2 \le \overline{\mathsf{V}} - 2\mathsf{X}_2$. Finally, we can conclude that (3.1) is a sufficient condition to guarantee (3.6) holds. The proof is accomplished.

Remark 3. *The power system under investigation is a complex continuous system, whose stabilization is further complicated by disturbances such as wind power generation, making the calculation of controller parameters a challenging task. Lyapunov theory is well used to facilitate analysis and predict system behavior, especially for complex systems.*

4. Simulation results

In this part, we consider a simulation example for a two-area power system and demonstrate the usefulness of this method. The parameter values of system (2.15) are shown in Table 2 [25].

Table 2. Parameters used in the two-area LFC schemes.

	T_t	T_g	R	D	β	M	c_p	m	k	d_{ac}	EER	T_{12}	T_W	T_{PC}
Area1	0.30	0.10	0.05	1.00	21.0	10	1.01	0.25	8	0.025	3.75	0.1968	0.30	0.30
Area2	0.40	0.17		1.50	21.5	12			15	0.015				

Set $\sigma = 0.01$, $d_M = 0.1$, $d_m = 0.02$ and the sampling period is $h = 0.05$. The initial condition, in this simulation analysis, is given by $\tilde{x}(0) = \begin{bmatrix} 0.001 & 0.001 & \dots & 0.001 \end{bmatrix}$. Next, by solving Theorem 2, the control gain $\mathcal{K}$ and the observer gain $\mathcal{L}$ are given by

$$\mathcal{K} = \begin{bmatrix} 0.0003 & -0.0074 & 0 & 0 & 0 & 0 & -0.0005 & 0.0003 & -0.0082 & 0 & 0 & 0 & 0 & 0.0011 \\ -0.0001 & 0.0016 & 0 & 0 & 0 & 0 & -0.0001 & -0.0001 & 0.0017 & 0 & 0 & 0 & 0 & -0.0002 \end{bmatrix},$$

$$\mathcal{L} = \begin{bmatrix} 0.0437 & 0.0547 & 0.0004 & -9.4284 & 0.0030 & 0.0030 & 0.0096 & -0.0012 & -0.0520 & 0.0003 & 0.0017 & 0 & 0 & 0.0061 \\ -0.0007 & -0.0516 & 0.0008 & 0.0981 & 0 & 0 & 0.0018 & 0.0365 & 0.0535 & -0.0129 & -0.1127 & 0.0021 & 0.0021 & 0.0186 \end{bmatrix}^T.$$

Meanwhile, H_∞ performance index $\gamma = 15.4285$. Here we set the disturbance $\omega(t)$ occurs at every sampling instant as $\omega(t) = \frac{\sqrt{0.16}}{1+t^2}$, and the probability that the system suffers from an effective DoS is 0.3.

In this simulation, we analyze the effects of a DoS attack on system dynamics and control responses.

Figure 2 illustrates DoS attack signals from $0 - 10$ s denoted by $\tau(i_k h)$, highlighting the attack's temporal characteristics and intervals of disrupted transmission.

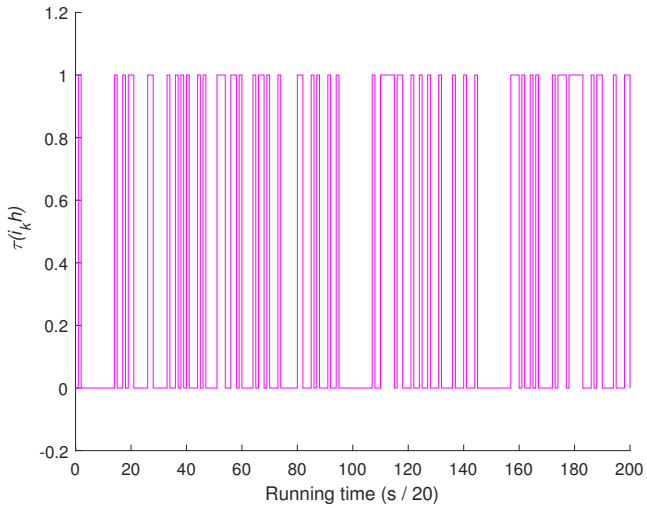

Figure 2. DoS attack signal $\tau(i_k h)$.

The frequency deviation Δf_i in the affected region, as depicted in Figure 3, shows fluctuations due to the DoS attack. However, it gradually stabilizes and tends toward zero, indicating a system tendency to regain frequency balance over time. This response underscores the system's capacity for frequency recovery even under compromised conditions.

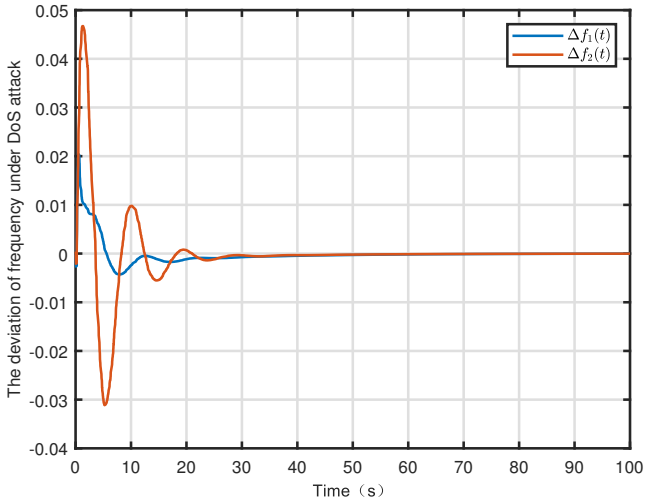

Figure 3. The frequency deviation Δf_i.

Figure 4 presents the output power deviation ΔP_{aci} of the ACs in the region under DoS attack. Notably, the fluctuations are contained within a narrow range, remaining below 0.1, demonstrating a limited impact on the output power deviation of the ACs. This outcome suggests that the control strategy maintains a relatively stable response in the face of attack-induced disturbances.

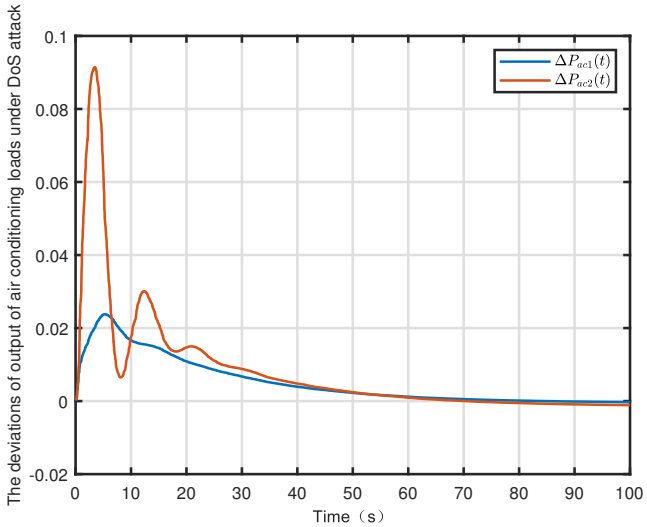

Figure 4. Output of ACs deviations ΔP_{aci}.

The area control error ACE_i in Figure 5 provides insights into area control performance under the DoS attack.

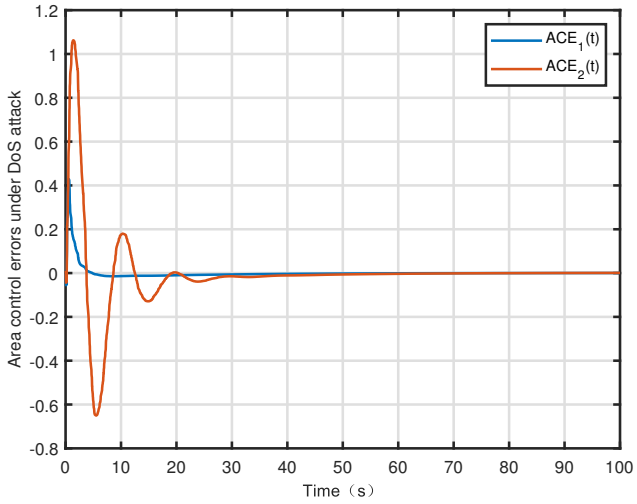

Figure 5. Area control error ACE_i.

Meanwhile, Figure 6 depicts the error between the observer state and the system state, revealing a similar pattern between them. While exhibiting oscillatory behavior, the rapid reduction of the error, however, is not completely zero due to the presence of perturbations. This suggests that the observer maintains some accuracy despite the attacks.

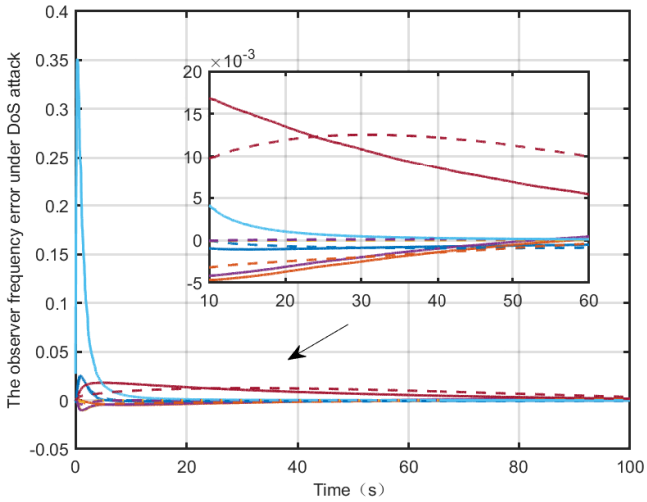

Figure 6. Observer frequency error.

The timing of event triggers, illustrated in Figure 7, reveals that the maximum trigger interval significantly exceeds the sampling period. This long trigger interval shows the efficacy of the proposed ETM in maintaining system stability and efficiency under DoS conditions. The extended trigger interval also highlights the ETM's capability to manage communication load, triggering transmissions only when essential and thus enhancing safety and stability in the presence of network-based attacks.

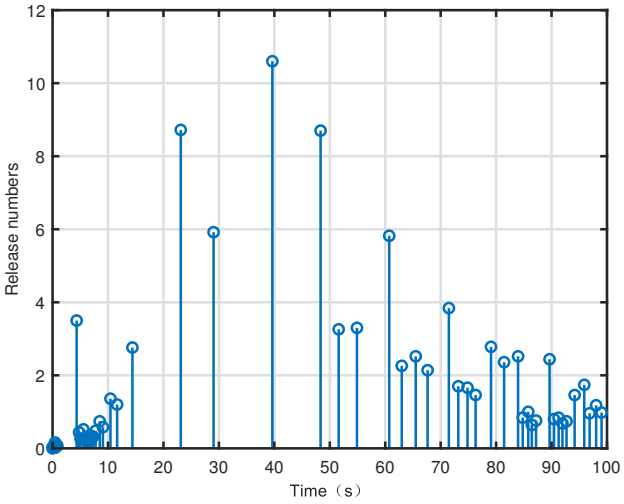

Figure 7. Release numbers.

5. Conclusions

In this paper, we have studied the problem of LFC with ACs under DoS attack considering ETM in network environment. When constructing the system model, we have considered the randomness of wind power generation and photovoltaic power generation and have also added the ACs to participate in the frequency regulation. In order to improve the utilization efficiency of network resources while resisting DoS attacks, an ETM has been proposed. During DoS attacks, system stability criteria and control design methods have been derived using H_∞ stability theory and LMI techniques for co-designing controller and observer gains. Finally, the proposed control strategy has been applied to the two-area smart grid, and the results have shown that the control method is effective.

Use of AI tools declaration

The authors declare they have not used Artificial Intelligence (AI) tools in the creation of this article.

Acknowledgments

This work was supported by Science and Technology Project of State Grid Anhui Electric Power Co., Ltd. (Grant No. 521205240016).

Conflict of interest

The authors declare there are no conflicts of interest.

References

1. C. Peng, J. Li, M. Fei, Resilient event-triggering H_∞ load frequency control for multi-area power systems with energy-limited dos attacks, *IEEE Trans. Power Syst.*, **32** (2016), 4110–4118. https://doi.org/10.1109/TPWRS.2016.2634122
2. Y. Güler, I. Kaya, Load frequency control of single-area power system with PI–PD controller design for performance improvement, *J. Electr. Eng. Technol.*, **18** (2023), 2633–2648. https://doi.org/10.1007/s42835-022-01371-1
3. J. C. Vinitha, G. Ramadas, P. U. Rani, PSO based fuzzy logic controller for load frequency control in EV charging station, *J. Electr. Eng. Technol.*, **19** (2024), 193–208. https://doi.org/10.1007/s42835-023-01568-y
4. Y. Xue, X. Lei, F. Xue, C. Yu, C. Dong, F. Wen, et al., Comment on the impact of wind power uncertainty on power system, *Proc. CSEE*, **34** (2014), 5029–5040. https://doi.org/10.13334/j.0258-8013.pcsee.2014.29.004
5. S. Wang, K. Tomsovic, Fast frequency support from wind turbine generators with auxiliary dynamic demand control, *IEEE Trans. Power Syst.*, **34** (2019), 3340–3348. https://doi.org/10.1109/TPWRS.2019.2911232
6. D. Katipoğlu, S. Soylu, Design of optimal FOPI controller for two-area time-delayed load frequency control system with demand response, *J. Electr. Eng. Technol.*, **19** (2024), 4073–4085. https://doi.org/10.1007/s42835-024-01900-0
7. V. Lakshmanan, M. Marinelli, J. Hu, H. W. Bindner, Provision of secondary frequency control via demand response activation on thermostatically controlled loads: solutions and experiences from denmark, *Appl. Energy*, **173** (2016), 470–480. https://doi.org/10.1016/j.apenergy.2016.04.054
8. Q. Zhu, L. Jiang, W. Yao, C. Zhang, C. Luo, Robust load frequency control with dynamic demand response for deregulated power systems considering communication delays, *Electr. Power Compon. Syst.*, **45** (2017), 75–87. https://doi.org/10.1080/15325008.2016.1233300
9. N. Li, X. Wang, Research of air conditioners providing frequency controlled reserve for microgrid, *Power Syst. Prot. Control*, **43** (2015), 101–105.
10. D. S. Callaway, Tapping the energy storage potential in electric loads to deliver load following and regulation, with application to wind energy, *Energy Convers. Manage.*, **50** (2009), 1389–1400. https://doi.org/10.1016/j.enconman.2008.12.012
11. N. Lu, D. P. Chassin, S. E. Widergren, Modeling uncertainties in aggregated thermostatically controlled loads using a state queueing model, *IEEE Trans. Power Syst.*, **20** (2005), 725–733. https://doi.org/10.1109/TPWRS.2005.846072
12. Z. Cai, Z. Zhang, Y. Yan, S. Liu, Multistage coordinated control risk dispatch considering the uncertainty of source-network, in *2022 4th International Conference on Power and Energy Technology (ICPET)*, (2022), 1305–1311. https://doi.org/10.1109/ICPET55165.2022.9918528
13. B. Pang, X. Jin, Q. Zhang, Y. Tang, K. Liao, J. Yang, et al., Transient ac overvoltage suppression orientated reactive power control of the wind turbine in the lcc-hvdc sending grid, *CES Trans. Electr. Mach. Syst.*, **8** (2024), 152–161. https://doi.org/10.30941/CESTEMS.2024.00020

14. T. Li, Y. Li, Y. Zhu, Research on the voltage supporting capability of multi-VSC-HVDC subsystems operation strategy to receiving-end LCC-HVDC network in weakAC grid, *CES Trans. Electr. Mach. Syst.*, **7** (2023), 11–20. https://doi.org/10.30941/CESTEMS.2023.00007

15. A. Kazemy, J. Lam, X. Zhang, Event-triggered output feedback synchronization of master–slave neural networks under deception attacks, *IEEE Trans. Neural Networks Learn. Syst.*, **33** (2020), 952–961. https://doi.org/10.1109/TNNLS.2020.3030638

16. X. Zhang, Q. Han, B. Zhang, X. Ge, D. Zhang, Accumulated-state-error-based event-triggered sampling scheme and its application to H_∞ control of sampled-data systems, *Sci. China Inf. Sci.*, **67** (2024), 162206. https://doi.org/10.1007/s11432-023-4038-3

17. R. Ji, S. S. Ge, Event-triggered tunnel prescribed control for nonlinear systems, *IEEE Trans. Fuzzy Syst.*, **32** (2023), 90–101. https://doi.org/10.1109/TFUZZ.2023.3290934

18. G. Zhang, S. Yin, C. Huang, W. Zhang, J. Li, Structure synchronized dynamic event-triggered control for marine ranching AMVs via the multi-task switching guidance, *IEEE Trans. Intell. Transp. Syst.*, 2024. https://doi.org/10.1109/TITS.2024.3463181

19. Y. Xiao, W. Che, Event-triggered fully distributed H_∞ containment control for MASs, *IEEE Trans. Syst. Man Cybern.: Syst.*, **54** (2024), 2676–2684. https://doi.org/10.1109/TSMC.2023.3342410

20. J. P. Farwell, R. Rohozinski, Stuxnet and the future of cyber war, *Survival*, **53** (2011), 23–40. https://doi.org/10.1080/00396338.2011.555586

21. D. Ding, Z. Wang, Q. Han, G. Wei, Security control for discrete-time stochastic nonlinear systems subject to deception attacks, *IEEE Trans. Syst. Man Cybern.: Syst.*, **48** (2016), 779–789. https://doi.org/10.1109/TSMC.2016.2616544

22. W. Xu, W. Trappe, Y. Zhang, T. Wood, The feasibility of launching and detecting jamming attacks in wireless networks, in *MobiHoc '05: Proceedings of the 6th ACM International Symposium on Mobile ad hoc Networking and Computing*, (2005), 46–57. https://doi.org/10.1145/1062689.1062697

23. H. S. Foroush, S. Martinez, On event-triggered control of linear systems under periodic denial-of-service jamming attacks, in *2012 IEEE 51st IEEE Conference on Decision and Control (CDC)*, (2012), 2551–2556. https://doi.org/10.1109/CDC.2012.6425868

24. C. De Persis, P. Tesi, Input-to-state stabilizing control under denial-of-service, *IEEE Trans. Autom. Control*, **60** (2015), 2930–2944. https://doi.org/10.1109/TAC.2015.2416924

25. L. Jin, Y. He, C. Zhang, X. Shangguan, L. Jiang, M. Wu, Equivalent input disturbance-based load frequency control for smart grid with air conditioning loads, *Sci. China Inf. Sci.*, **65** (2022), 122205. https://doi.org/10.1007/s11432-020-3120-0

26. D. Yue, E. Tian, Q. Han, A delay system method for designing event-triggered controllers of networked control systems, *IEEE Trans. Autom. Control*, **58** (2012), 475–481. https://doi.org/10.1109/TAC.2012.2206694

27. X. Zhang, Q. Han, B. Zhang, An overview and deep investigation on sampled-data-based event-triggered control and filtering for networked systems, *IEEE Trans. Ind. Inf.*, **13** (2016), 4–16. https://doi.org/10.1109/TII.2016.2607150

28. W. P. M. H. Heemels, M. C. F. Donkers, A. R. Teel, Periodic event-triggered control for linear systems, *IEEE Trans. Autom. Control*, **58** (2012), 847–861. https://doi.org/10.1109/TAC.2012.2220443

29. H. Zhang, J. Liu, S. Xu, H-infinity load frequency control of networked power systems via an event-triggered scheme, *IEEE Trans. Ind. Electron.*, **67** (2019), 7104–7113. https://doi.org/10.1109/TIE.2019.2939994

30. C. De Persis, P. Tesi, Resilient control under denial-of-service, *IFAC Proc. Volumes*, **47** (2014), 134–139. https://doi.org/10.3182/20140824-6-ZA-1003.02184

31. K. Lu, G. Zeng, X. Luo, J. Weng, Y. Zhang, M. Li, An adaptive resilient load frequency controller for smart grids with DoS attacks, *IEEE Trans. Veh. Technol.*, **69** (2020), 4689–4699. https://doi.org/10.1109/TVT.2020.2983565

32. Y. Qi, S. Yuan, B. Niu, Asynchronous control for switched T–S fuzzy systems subject to data injection attacks via adaptive event-triggering schemes, *IEEE Trans. Syst. Man Cybern.: Syst.*, **52** (2021), 4658–4670. https://doi.org/10.1109/TSMC.2021.3100481

33. H. Sun, C. Peng, D. Yue, Y. L. Wang, T. Zhang, Resilient load frequency control of cyber-physical power systems under QoS-dependent event-triggered communication, *IEEE Trans. Syst. Man Cybern.: Syst.*, **51** (2020), 2113–2122. https://doi.org/10.1109/TSMC.2020.2979992

34. E. Tian, K. Wang, X. Zhao, S. Shen, J. Liu, An improved memory-event-triggered control for networked control systems, *J. Franklin Inst.*, **356** (2019), 7210–7223. https://doi.org/10.1016/j.jfranklin.2019.06.041

35. C. Peng, S. Ma, X. Xie, Observer-based non-PDC control for networked T–S fuzzy systems with an event-triggered communication, *IEEE Trans. Cybern.*, **47** (2017), 2279–2287. https://doi.org/10.1109/TCYB.2017.2659698

AIMS Press